Catena 175 (2019) 263–277

Contents lists available at ScienceDirect

Catena

journal homepage: www.elsevier.com/locate/catena

Assessing landslide characteristics in a changing climate in northern Taiwan

Chi-Wen Chen[a,b,*], Yu-Shiang Tung[a], Jun-Jih Liou[a], Hsin-Chi Li[a], Chao-Tzuen Cheng[a], Yung-Ming Chen[a], Takashi Oguchi[b]

[a] National Science and Technology Center for Disaster Reduction, No. 200, Sec. 3, Beixin Road, Xindian District, New Taipei City, Taiwan
[b] Center for Spatial Information Science, The University of Tokyo, 5-1-5 Kashiwanoha Kashiwa, Chiba 277-8568, Japan

ARTICLE INFO

Keywords:
Climate change
Dynamical downscaling
Landslide
Rainfall
Empirical relationship
Recurrence interval

ABSTRACT

This study analyzed landslide characteristics under extreme precipitation with regard to present and future scenarios, in order to analyze the effects of climate change on landslide activities. For our study area, we selected two adjacent catchments in northern Taiwan: the Shihmen Reservoir catchment, an area with high-relief topography that is susceptible to landslides at present, and the Xindian River catchment, an area with gentle topography that is not prone to landslides at present. This study established empirical relationships between landslide-area characteristics and rainfall conditions according to rainfall-induced landslides during past typhoon events. The relationships were applied to estimate landslide-area characteristics caused by typhoon events for the base period (1979–2003) and the end of the 21st century (2075–2099) according to the climate change scenario of representative concentration pathways 8.5 (RCP8.5) and dynamical downscaling of rainfall data in Taiwan. We also analyzed rainfall amounts at different recurrence intervals from different rainfall durations for the two catchments. We found that the area with high-relief topography (the Shihmen Reservoir catchment) is relatively prone to landslides currently and that the cumulative rainfall is a key factor controlling landslide-area characteristics. On the other hand, the area with gentle topography (the Xindian River catchment) is less prone to landslides at present, and the rainfall intensity is a key factor controlling landslide-area characteristics. Under the effects of climate change in the near future, both landslide severity and landslide frequency will increase more in areas with gentle topography than in areas with high-relief topography, in response to the more frequent occurrence of a strong typhoon with higher rainfall intensity.

1. Introduction

Landslides are a common natural hazard in mountainous areas worldwide. Even though the mechanism of landslides is very complicated, the most common triggering factor is extreme rainfall (Larsen and Simon, 1993; Crozier, 1999; Glade et al., 2000; Khan et al., 2012; Saito and Matsuyama, 2012; Oku et al., 2014). Therefore, many previous studies have tried to establish the relationship between rainfall conditions and landslide characteristics and used empirical models to assess a possible landslide scale under different conditions of heavy rainfall. Among the early studies, Uchiogi (1971) compared the average cumulative rainfall of a catchment with the landslide-area ratio to establish the relationship between them, thereby obtaining the critical rainfall that caused landslides. In recent years, many studies in Taiwan have also used this kind of empirical model to assess landslides in a catchment. For example, Shou et al. (2011) investigated the behavior of landslides in Central Taiwan after 1999 for the Ta-Chia River, the Wu River and the Chuo-Shuei River. They considered landslides triggered by four typhoons, Toraji in 2001, Mindulle in 2004, Sinlaku in 2008, and Morakot in 2009, to establish the empirical relationship between landslide-area ratio and average cumulative rainfall for those catchments. They found that the impact of the 1999 Chi-Chi earthquake on landslides triggered by subsequent typhoons decayed to 50% in about one to three years and to 10% in about ten years. In addition, Liu et al. (2013) further discussed the impact of the 1999 Chi-Chi earthquake by combining an empirical model with a statistical model to analyze changes in landslides from 1996 to 2008 in the Chuo-Shuei River catchment. Chou et al. (2017) analyzed the coastal alluvial fan in Suao, Taiwan, formed by landslide materials transported during Typhoon Megi in 2010, to establish an empirical model to assess the proportions of new landslides in the upstream area under different cumulative rainfalls. Similar empirical models have been widely used all over the world. Zhu et al. (2011) analyzed loose materials sourced from landslides caused by the 2008 Wenchuan earthquake in China and transformed into debris flows by subsequent torrential rain events, and explored the relationship between rainfall conditions and landslide area

* Corresponding author at: National Science and Technology Center for Disaster Reduction, No. 200, Sec. 3, Beixin Road, Xindian District, New Taipei City, Taiwan.
E-mail address: cwchen@csis.u-tokyo.ac.jp (C.-W. Chen).

https://doi.org/10.1016/j.catena.2018.12.023
Received 27 March 2018; Received in revised form 3 December 2018; Accepted 14 December 2018
Available online 21 December 2018
0341-8162/ © 2018 Elsevier B.V. All rights reserved.

using an empirical model combined with rainfall recurrence intervals. Their results show that the torrential rain events of the 50-year and 100-year recurrence intervals will likely generate 0.87 and 1.67 km^2 of new landslide area, respectively. Although the simplicity of the empirical approach neglects important hydrological controls, it offers a straightforward means for identifying regional-scale landslide characteristics based solely on rainfall data. The above-mentioned previous studies all established the empirical relationship between rainfall conditions and landslide characteristics based on cumulative rainfall; however, many studies have pointed out that mean rainfall intensity and peak rainfall intensity are also closely related to the occurrence of landslides (Aleotti, 2004; Dahal and Hasegawa, 2008; Chen et al., 2015). In addition, the relationship between rainfall intensity and duration, called the *I–D* relationship, is commonly used as an indicator to assess the occurrence of landslides in studies of rainfall-induced landslides (Caine, 1980; Guzzetti et al., 2007, 2008; Brunetti et al., 2010; Saito et al., 2010; Chen et al., 2015). In these studies, the *I–D* relationship was used to find the rainfall threshold for landslides, such as 2% or 5% of the lower bound determined by statistical methods including the Bayesian inference method, the quantile-regression method, and the frequentist method (Guzzetti et al., 2007; Brunetti et al., 2010; Saito et al., 2010).

Another important aspect of landslides is their frequency of occurrence. The recurrence interval of rainfall conditions that trigger landslides is often used to determine the frequency of landslides. Iida (2004) studied the recurrence intervals of rainfall conditions associated with shallow landslides in the area east of Hamada in Shimane Prefecture, Japan. Heavy rainfall (about 350 mm in 6 h) on 15 July 1988 triggered many shallow landslides in that area, and he found that rainfall events with recurrence intervals of < 500 years and < 1000 years respectively trigger about 50% and 65% of the total number of landslides over the long term. On the other hand, Saito and Matsuyama (2015) produced a preliminary high-resolution probable hourly precipitation and probable Soil Water Index (SWI) for a 50-year recurrence interval over the Japanese archipelago from 5-km grid-cell radar/raingauge-analyzed precipitation with a 26-year time series (1988–2013). Their results revealed detailed spatial patterns of the probable hourly precipitation and SWI with a 5-km grid-cell, which enabled nationwide landslide hazard assessment.

In addition to the triggering factor, geomorphological and geological conditions are also very important factors in the landslide occurrence (Yalcin, 2008) and are often used to determine the susceptibility of an area to landslides (e.g., Ayalew and Yamagishi, 2005). The bedrock geology is highly related to the occurrence of landslides, which may or may not favor displacements along well-defined shearing surfaces (Migoń et al., 2017). Among the geomorphological factors, elevation, slope, and aspect are commonly used in landslide research as they have different significances in the occurrence of landslides (e.g., Guzzetti et al., 1999; Paudel et al., 2016) Varied geomorphologic and geologic conditions in different areas cause differences in the effects of typhoons on landslide occurrence and characteristics.

Climate change is an important issue that has attracted growing attention in recent years. The report of the International Panel on Climate Change (IPCC) noted that rises in temperature and sea level are ongoing and that appropriate adaptations to reduce disaster risk are necessary (IPCC, 2007). In the current changing environment, both the probability of the occurrence of a strong typhoon and the rainfall intensity during a typhoon event will increase (Emanuel, 2005; Webster et al., 2005; Tu et al., 2009). Many studies have explored the potential effects of different climate change scenarios on slope disasters (Melchiorre and Frattini, 2012; Turkington et al., 2016). According to the Taiwan climate change report, the frequency of extreme rainfall events has also increased in the past 20 years in Taiwan (Hsu et al., 2011). Taiwan is extremely susceptible to landslides because of its steep mountainous topography and frequent heavy rainfall and earthquakes (Chen et al., 1999; Chen and Su, 2001; Dadson et al., 2003; Chuang et al., 2009). Under the impact of climate change, extreme rainfall events will become more frequent, and the possibility of landslides in the upstream area will increase significantly. These disasters will result in considerable losses of life and property. However, there is almost no study addressing the effect of climate change on landslides in Taiwan. Therefore, the objectives of this study are to establish the empirical relationship between rainfall conditions and landslide characteristics for two catchments in northern Taiwan using historical cases and to assess changes in the characteristics and frequency of landslides from the base period (1979–2003) to the end of the 21st century (2075–2099) according to the climate change scenario and dynamical downscaling of rainfall data in Taiwan. We also discussed differences in geomorphologic and geologic conditions between the two catchments, relating to landslide characteristics at present and under future climates. These results not only provide a reference for areas having similar climate change trends over the world, but also open the possibility to analyze characteristics and frequency of landslides under climate change scenarios from triggering and predisposing factors.

2. Study area

The Tamsui River Basin covers the metropolitan regions of Taipei City, New Taipei City, Keelung City, and Taoyuan City (Fig. 1a). The Tamsui River is the third longest river in Taiwan, having a total length of about 159 km and a drainage area of 2726 km^2. The total population in this metropolitan area is over seven million. The Dahan River and Xindian River flow toward the northeast and northwest respectively before successively merging into the Tamsui River, which is the major river in this basin and flows northwestward into the Taiwan Strait. According to the river flow observation in 2012 (Taiwan Water Resources, 2013), the average flow fluxes in the Dahan River and Xindian River were approximately 40 and 62 m^3/s, respectively. In this study, we chose two catchments in the upstream area of the Tamsui River Basin: the Shihmen Reservoir catchment (the Dahan River) and the Xindian River catchment. Fig. 1 shows the locations of the two catchments and their geomorphologic, land use, and geologic characteristics. Most areas of the two catchments are forested, without strong man-made interference. The majority of the two catchments is composed of Paleogene to Neogene sedimentary rocks and metamorphic rocks, and Quaternary deposits. Fig. 2 shows that in the Shihmen Reservoir catchment, the elevation ranges from 206 to 3523 m, with an average of 1408 m, and the slope ranges from 0 to 86.4°, with an average of 33.3°. In the Xindian River catchment, the elevation ranges from 0 to 2130 m, with an average of 667 m, and the slope ranges from 0 to 89.5°, with an average of 28.7° (Fig. 2a, b). The proportions of slope aspects of the two catchments in all directions are almost the same within the range of 11–15% (Fig. 2c). The lithological conditions of the two catchments are also very similar in that most of the area is underlain by mudstone and sandstone, while a few areas are composed of metamorphic rock (Fig. 2d). The detailed description of the two catchments is given below.

2.1. Shihmen Reservoir catchment

The Shihmen Reservoir, completed in June 1964, is the largest water storage basin in northern Taiwan. It is located on the lower part of the Dahan River at 24.812°N and 121.247°E. The effective water storage capacity of the Shihmen Reservoir is about 2.7×10^8 m^3, and the water is mainly supplied by the Dahan River. During the construction of the Shihmen Reservoir, the 1963 typhoon Gloria caused considerable sediment yields, including 1.95×10^7 m^3 of sediment that settled at the bottom of the reservoir and occupied 7.2% of the water storage capacity (Chanson, 1998). The exceptionally high turbidity triggered by settled sediment and the reduction of the effective water storage capacity are potential problems for the Shihmen Reservoir.

The area of the Shihmen Reservoir catchment is about 760 km^2,

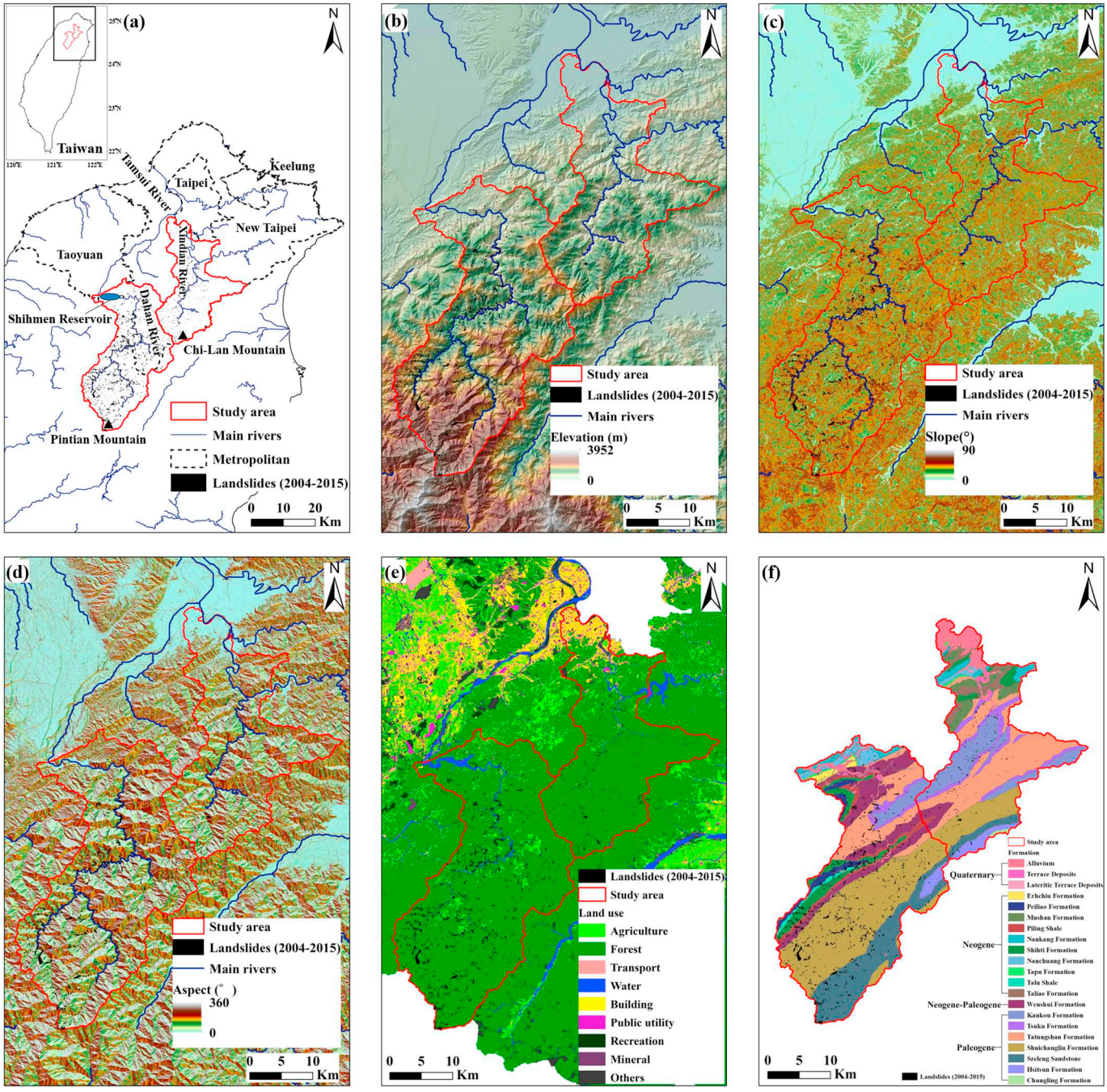

Fig. 1. Study area with (a) metropolitan area and landslides during 2004–2015, (b) elevation, (c) slope, (d) aspect, (e) land use, and (f) geology.

covering latitudes from 24.426°N to 24.861°N and longitudes from 121.192°E to 121.479°E, and it is composed of rugged topography with elevations ranging from 206 to 3523 m (Fig. 1b). About 80% of the slopes range from 30° to 50°, and the relief gradually slopes down from southeast to northwest (Fig. 1c). Tectonic features can be seen from the presence of faults, folds, and fissures, which are distributed throughout the catchment, mostly along the northeast–southwest direction. Lin et al. (2007) pointed out that the discontinuity density averages 19.2 m^{-3} for the rock formations in the catchment area, indicating that the rock mass on the hillslope is considerably fractured. The bedrock in the catchment has strikes of N30°E to N60°E and southward dips of 35° to 70° (Lin et al., 2011). In the lower catchment, the major lithology is composed of alternations of sandstone and shale. The middle catchment is underlain by argillite, sandy shale, and slate. In the upper catchment are heavily deformed and complex formations occur consisting of argillite, slate, massive sandstone, alternations of shale and sandstone, and thick-bedded meta-sandstone (Fig. 1f).

The Shihmen Reservoir catchment has a subtropical-monsoon climate, affected by typhoons in summer and the NE monsoon in winter. The average temperature is about 20 °C and the average humidity is about 82%. The annual precipitation averages 2556 mm and is highly concentrated during the typhoon season, which is from May to September.

2.2. Xindian River catchment

The Xindian River, located in the northern part of Taiwan, is one of the major tributaries of the Tamsui River, which flows through New Taipei City and Taipei City (Huang et al., 2012). The Xindian River is 45 km long and has a drainage area of 490 km^2. It originates from Chi-

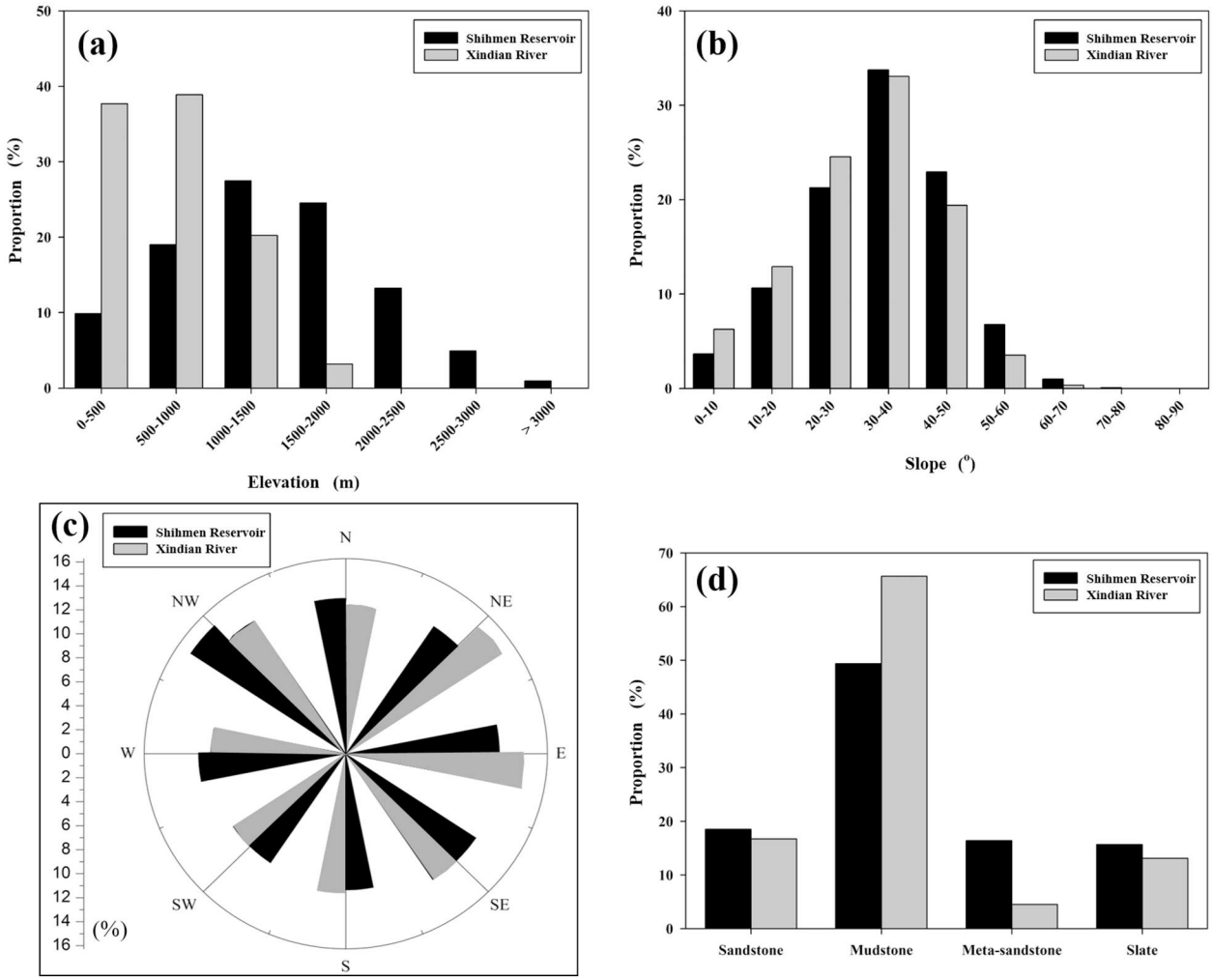

Fig. 2. Comparisons between the two catchments: (a) elevation, (b) slope, (c) aspect, and (d) main lithology.

Lan Mountain (elevation of 2130 m) and flows in the deep valley toward the north (Hu et al., 2007).

Most of the bedrock in this catchment experienced slight metamorphism, and the degree of metamorphism increases from northwest to southeast with the strike in the northeast direction. The major lithology is composed of gravel, muddy sand, shale, argillite, and slate (Fig. 1f; Ho, 1986; Teng, 1990). The Xindian River catchment with a subtropical-monsoon climate is affected by typhoons in summer and the NE monsoon in winter. For areas of elevation < 500 m, the average temperature is about 28 °C in July and 13 °C in January. For areas of elevation > 1000 m, the average temperature is about 20 °C in summer and 6 °C in winter. The annual precipitation averages 3000–4000 mm and is highly concentrated during the typhoon season, which is from May to September (Shieh, 2000).

3. Data and methods

3.1. Landslide-area characteristics

The Forestry Bureau of Taiwan identifies the landslide inventory for all of Taiwan using satellite images in the first half (January to June) of each year (https://www.tgos.tw/TGOS/Web/Metadata/TGOS_MetaData_View.aspx?MID=CDBB21ACB7275BDB56E94ED8BA9E9546&SHOW_BACK_BUTTON=false&keyword=). The landslide inventory is automatically interpreted according to the operating standards set by the Forestry Bureau, and the minimum area of a landslide is 0.1 ha. According to the classification of landslides developed by Varnes (1978), all these landslides belong to the category of slide (rotational and translational) types. This study collected the landslide inventories of a 12-year period from 2004 to 2015 and extracted the landslide events in the Shihmen Reservoir catchment and the Xindian River catchment (Fig. 1). In addition, we selected eight typhoons, which were at least medium-strength typhoons according to the classification system of the Central Weather Bureau of Taiwan (CWB) and had tracks that passed through northern Taiwan, for analysis of the landslide-area characteristics (Fig. 3). The eight typhoons were Typhoon Aere (August 2004), Typhoon Matsa (August 2005), Typhoon Krosa (October 2007), Typhoon Sinlaku (September 2008), Typhoon Morakot (August 2009), Typhoon Saola (July–August 2012), Typhoon Soulik (July 2013), and Typhoon Soudelor (August 2015). These typhoons, which we have carefully checked the precipitation in northern Taiwan, were the most influential rainfall events in the study area during each period. Therefore, the landslide inventory identified after one typhoon event can represent the effects of the typhoon event on the landslide distributions of the two catchments. Although some relatively small rainfall events in each period may have caused landslides, the data set cannot easily present this kind of information. As the best way to use the data set, we assumed that all landslides were caused by the worst typhoon during a period, and calculated the landslide-area characteristics after each typhoon event for the two catchments, including the maximum landslide area, number of landslides, total landslide area, and landslide-area ratio. In addition, we also analyzed geological and geomorphological features of landslides according to their locations in the two catchments.

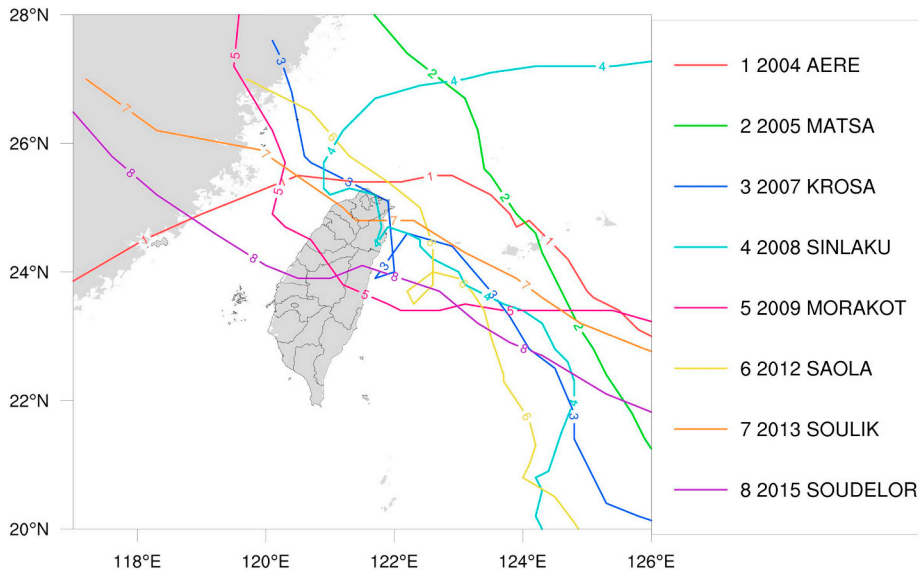

Fig. 3. The eight historical typhoon tracks.

Table 1
Landslide-area characteristics during each typhoon event of the two catchments.

Typhoon event	Number of landslides		Maximum landslide area (m^2)		Total landslide area (km^2)		Landslide-area ratio (%)	
	Shihmen	Xindian	Shihmen	Xindian	Shihmen	Xindian	Shihmen	Xindian
2004 Aere	769	109	6.06×10^5	4.24×10^4	4.89	0.36	0.65	0.074
2005 Matsa	537	45	6.05×10^5	3.35×10^4	3.80	0.19	0.50	0.040
2007 Krosa	356	58	4.13×10^5	1.99×10^4	3.85	0.22	0.51	0.044
2008 Sinlaku	251	29	9.36×10^4	2.67×10^4	1.29	0.10	0.17	0.020
2009 Morakot	442	21	2.17×10^5	2.62×10^4	3.26	0.10	0.43	0.020
2012 Saola	359	16	2.49×10^5	8.16×10^4	1.99	0.15	0.26	0.031
2013 Soulik	349	16	2.21×10^5	3.23×10^4	2.01	0.08	0.27	0.015
2015 Soudelor	N/A	164	N/A	1.17×10^5	N/A	0.65	N/A	0.132

Table 2
Average rainfall conditions of catchments during each typhoon event.

Typhoon event	Cumulative rainfall (mm)		Rainfall duration (h)		Mean rainfall intensity (mm/h)		Peak rainfall intensity (mm/h)	
	Shihmen	Xindian	Shihmen	Xindian	Shihmen	Xindian	Shihmen	Xindian
2004 Aere	859.48	530.75	40.00	40.00	21.49	13.27	47.04	31.97
2005 Matsa	729.14	517.38	37.00	34.00	19.71	15.22	35.63	34.52
2007 Krosa	619.98	611.42	42.00	44.00	14.76	13.90	34.77	32.89
2008 Sinlaku	981.85	1099.07	70.00	87.00	14.03	12.63	34.43	41.20
2009 Morakot	419.09	306.62	37.00	38.00	11.33	8.07	37.81	32.28
2012 Saola	849.20	680.13	72.00	68.00	11.79	10.00	44.88	54.43
2013 Soulik	379.16	179.35	18.00	13.00	21.06	13.80	70.19	24.66
2015 Soudelor	N/A	509.48	N/A	25.00	N/A	20.38	N/A	48.88

3.2. Rainfall events

To analyze rainfall conditions during the eight typhoons, this study used the estimated rainfall based on integrated radar-gauge data (KRID) produced by the National Science and Technology Center for Disaster Reduction of Taiwan (NCDR). The KRID is obtained from the data of radar reflectivity and corrected by observation data of rain gauges, with spatial and temporal resolutions of 0.0125° per hour. A continuous rainfall event is considered to begin when hourly rainfall surpasses 4 mm and ends when hourly rainfall falls below 4 mm over the next 6 consecutive hours (e.g., Chang et al., 2011; Chen et al., 2015). Employing the above definition, this study identified the rainfall events and calculated the average rainfall conditions during each typhoon period for the Shihmen Reservoir catchment and the Xindian River catchment, including cumulative rainfall (E; mm), rainfall duration (D; h), mean rainfall intensity (I; mm/h), and peak rainfall intensity (I_p; mm/h). The average rainfall conditions during each typhoon period of the two catchments were compared with the maximum landslide area, number of landslides, total landslide area, and landslide-area ratio induced by each typhoon to establish the empirical relationship between rainfall conditions and landslide-area characteristics.

3.3. I–D relationship of landslides

The method used to determine the I–D relationship is to plot the mean rainfall intensities and rainfall durations of all landslides, calculated from the beginning of the rainfall event to the occurrence of landslides, on an X-Y logarithm coordinate and to find the correlation

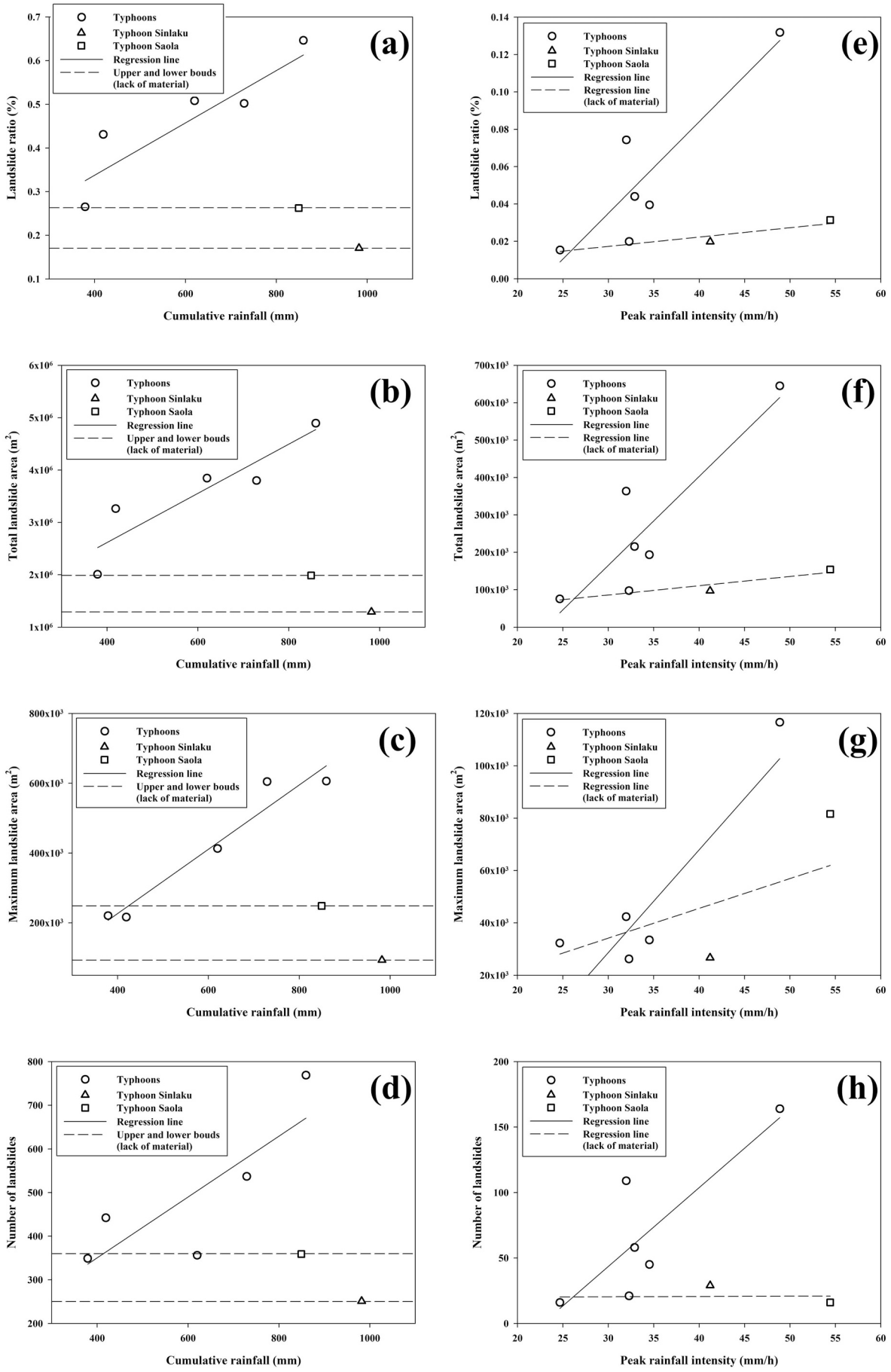

(caption on next page)

Fig. 4. Average rainfall conditions with landslide-area characteristics during the typhoon events of the two catchments. Cumulative rainfall vs. (a) landslide ratio, (b) total landslide area, (c) maximum landslide area, and (d) number of landslides for the Shihmen Reservoir catchment. Peak rainfall intensity vs. (e) landslide ratio, (f) total landslide area, (g) maximum landslide area, and (h) number of landslides for the Xindian River catchment.

Table 3
Pearson correlation coefficient matrix for rainfall conditions and landslide-area characteristics during typhoon events in the Shihmen Reservoir catchment. *D*: rainfall duration; *E*: cumulative rainfall; *I*: mean rainfall intensity; I_p: peak rainfall intensity; A_M: maximum landslide area; *L*: landslide-area ratio; *N*: number of landslides; A_T: total landslide area.

	D	*E*	*I*	I_p	A_M	*L*	*N*	A_T
D	1.00							
E	0.65	1.00						
I	−0.40	0.44	1.00					
I_p	−0.91	−0.43	0.57	1.00				
A_M	0.57	0.97	0.50	−0.42	1.00			
L	0.86	0.91	0.07	−0.63	0.81	1.00		
N	0.43	0.82	0.45	−0.17	0.74	0.79	1.00	
A_T	0.86	0.91	0.07	−0.63	0.81	1.00	0.79	1.00

Table 4
Pearson correlation coefficient matrix for rainfall conditions and landslide-area characteristics during typhoon events in the Xindian River catchment. *D*: rainfall duration; *E*: cumulative rainfall; *I*: mean rainfall intensity; I_p: peak rainfall intensity; A_M: maximum landslide area; *L*: landslide-area ratio; *N*: number of landslides; A_T: total landslide area.

	D	*E*	*I*	I_p	A_M	*L*	*N*	A_T
D	1.00							
E	0.70	1.00						
I	−0.36	0.40	1.00					
I_p	0.07	0.52	0.69	1.00				
A_M	−0.35	0.18	0.79	0.87	1.00			
L	0.00	0.54	0.79	0.89	0.91	1.00		
N	0.06	0.57	0.75	0.84	0.86	0.99	1.00	
A_T	0.00	0.54	0.79	0.89	0.91	1.00	0.99	1.00

between them. It also captures every landslide affected by antecedent rainfall conditions, which are reflected in the *I–D* conditions that caused the landslide. However, we have no way to know the exact occurrence time of each landslide from the landslide inventories. A previous study has pointed out that about 75% Taiwan's recorded landslides occurred close to the time of peak rainfall intensity, except for some landslides triggered by a very large or very small amount of cumulative rainfall (Chen et al., 2015). Therefore, we excluded the highest and lowest 12.5% of landslides according to the cumulative rainfall during a rainfall event and assumed that the remaining 75% of the landslides occurred at the time of peak rainfall intensity. Based on the above assumptions, we calculated the mean rainfall intensity (I_b; mm/h) and rainfall duration (D_b; h) of each landslide from the beginning of the rainfall event to the occurrence of landslides. This study focused on the regression line of the *I–D* relationship, which represents the overall trend of rainfall conditions for landslides in the two catchments. To establish the *I–D* relationship from the landslide inventories, this study used I_b and D_b of each landslide, and the *I–D* relationship can be expressed by the following formula (Caine, 1980):

$$I_b = \alpha D_b^{-\beta} \tag{1}$$

where α is a scaling constant (intercept), and β is the shape parameter (slope).

3.4. Recurrence intervals of extreme rainfall

Recurrence intervals and values are common methods used in extreme-value frequency analysis of hydrological statistics. In this study, we used hourly rainfall data from rain gauges distributed around Taiwan during a 23-year period from 1991 to 2013 and adopted kriging interpolation to obtain the mesh data with a resolution of 5 km. Many other interpolation methods, such as the spline and IDW (Inverse Distance Weighting) methods, are available, and different areas require different methods (Tao et al., 2009). However, deciding the best method for an area is quite difficult. For this reason, we chose kriging interpolation, which is commonly used in Taiwan for gauged rainfall estimates (Chiang and Chang, 2009; Chen et al., 2015). We estimated extreme rainfall values at different recurrence intervals (5-, 20-, 25-, and 50-year intervals) from different rainfall durations (2, 24, 48, and 72 h) for the two catchments. The maximum annual cumulative rainfall was extracted for different durations, which meets the maximum likelihood method (Kharin and Zwiers, 2005), and applied to the generalized extreme value distribution (GEV), which was used for calculating extreme rainfall at different recurrence intervals as below:

$$F(x;\mu,\sigma,\xi) = \begin{cases} e^{-e^{-\frac{x-\mu}{\sigma}}}, & \xi = 0 \\ e^{-\left\{1+\xi\frac{x-\mu}{\sigma}\right\}^{-\xi^{-1}}}, & 1+\xi\dfrac{x-\mu}{\sigma} > 0 \end{cases} \tag{2}$$

where ξ is a shape parameter, σ is a scaling parameter (slope), and μ is a location parameter.

3.5. Landslide characteristics under climate change

The resolution of the general circulation model (GCM) used for climate estimation and simulation is usually 100–200 km. It is difficult to identify the structure of a typhoon with a radius of less than several hundred kilometers. Owing to the low spatial resolution of the model, it is impossible to reasonably simulate the extreme weather system with a physical model, and it is impossible to carry out extreme weather estimation under climate change. (Roble and Ridley, 1994; Johns et al., 1997). Therefore, this study used a climate projection simulated from the high-resolution (approximately 20-km horizontal resolution) atmospheric general circulation model (AGCM) developed by the Meteorological Research Institute (MRI) under the Japan Meteorological Agency (JMA; Mizuta et al., 2012). The low boundary drive by ensemble mean sea surface temperature (SST) of the climate change scenario of representative concentration pathways 8.5 (RCP8.5) in Coupled Model Intercomparison Project Phase 5 (CMIP5; Mizuta et al., 2014) is called MRI-AGCM. This model has been validated for the simulation of typhoon generation (Murakami et al., 2012, 2014). However, the 20-km horizontal resolution still could not necessarily reflect the precipitation intensity caused by topographical effects in Taiwan. Therefore, the MRI-AGCM data were dynamically downscaled using the Weather Research and Forecasting Model (WRF), proposed by the US National Center for Atmospheric Research (NCAR), to obtain more realistic rainfall data for Taiwan with spatial and temporal resolutions of 5 km per hour.

Based on the downscaled rainfall data, there were 87 typhoons during the base period (1979–2003) and will be 43 typhoons in the last quarter of the 21st century. We selected eight typhoons in the base period and four typhoons at the end of the century, which accounted for the top 10% of the total rainfall for the Tamsui River Basin among all typhoons in the two periods, to discuss the impact of climate change on landslides. We calculated the rainfall conditions, including cumulative rainfall, rainfall duration, mean rainfall intensity, and peak rainfall intensity, of those typhoon events according to the definition of a rainfall event. The empirical relationships between rainfall conditions and landslide-area characteristics of the Shihmen Reservoir catchment and the Xindian River catchment were used to estimate the landslide-

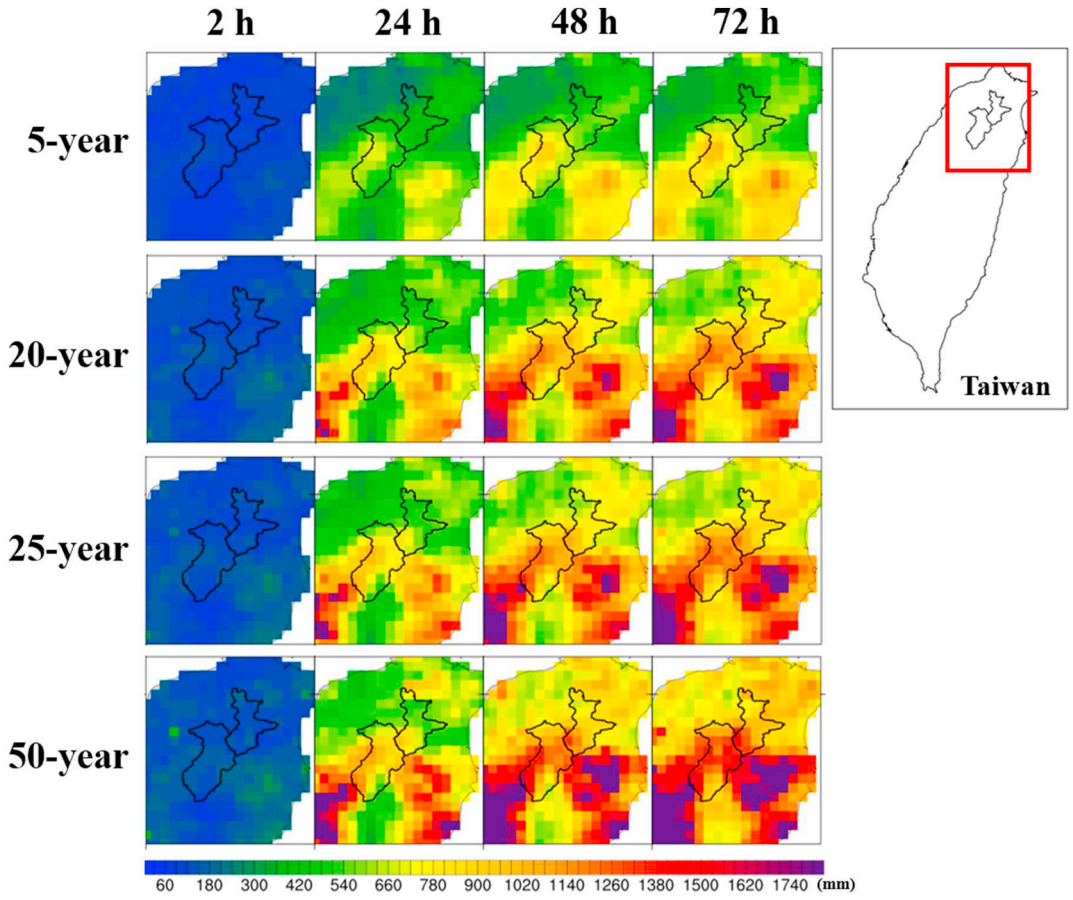

Fig. 5. Cumulative rainfall at different recurrence intervals from different rainfall durations estimated by using the interpolation rain gauge data from 1991 to 2013. The top-right map shows the range of each map and the relative locations of the two catchments.

Table 5
Rainfall conditions for landslides of the two catchments.

Catchment	Cumulative rainfall (mm)			Rainfall duration (h)			Mean rainfall intensity (mm/h)		
	Avg.	Max.	Min.	Avg.	Max.	Min.	Avg.	Max.	Min.
Shihmen Reservoir (n = 2297)	415.67	677.69	115.77	24.63	63.00	5.00	18.70	37.23	6.00
Xindian River (n = 344)	397.88	647.40	160.90	23.07	59.00	7.00	18.13	35.54	7.79

Table 6
Mean rainfall intensity at different recurrence intervals and different rainfall durations of the two catchments.

Recurrence interval (year)	2 h mean intensity (mm/h)		24 h mean intensity (mm/h)		48 h mean intensity (mm/h)		72 h mean intensity (mm/h)	
	Shihmen	Xindian	Shihmen	Xindian	Shihmen	Xindian	Shihmen	Xindian
5	51.27	48.29	21.54	17.54	13.82	11.45	9.91	8.25
20	66.67	60.15	30.34	24.42	20.06	16.45	14.47	11.91
25	69.12	61.94	31.67	25.48	21.05	17.24	15.20	12.50
50	76.86	67.46	35.77	28.77	24.20	19.70	17.56	14.32

area characteristics caused by the top 10% of typhoon events in the base period and the last quarter of the 21st century. In addition, this study also examined changes in the landslide frequencies of the two catchments from the base period to the end of the 21st century. We also used the same downscaled rainfall data to estimate the recurrence intervals and values of rainfall during the base period and the end of the 21st century for the two catchments respectively.

4. Results and discussion

4.1. Rainfall conditions and area characteristics of landslides

Table 1 shows the landslide-area characteristics of the two catchments after each typhoon event. For the Shihmen Reservoir catchment, Typhoon Aere in 2004 had the largest effect, resulting in 769 landslides, a maximum landslide area of 6.06×10^5 m^2, a total landslide area of 4.89 km^2, and a landslide-area ratio of 0.65%. The smallest effect was during Typhoon Sinlaku in 2008, which resulted in 251 landslides, a

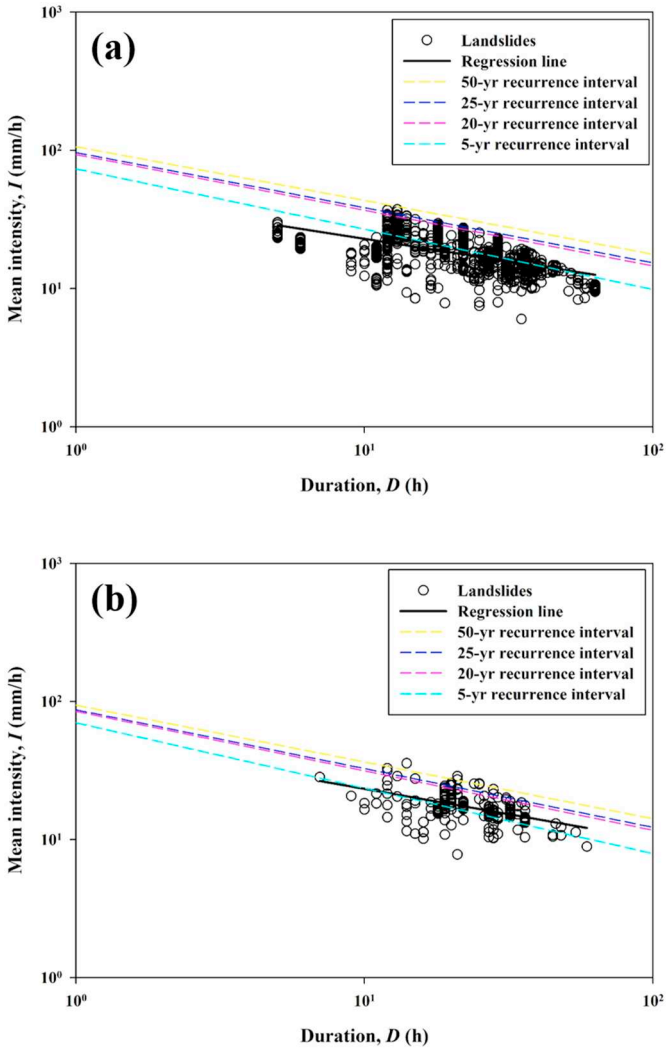

Fig. 6. *I–D* relationships of landslides and rainfall conditions at different recurrence intervals in (a) the Shihmen Reservoir catchment and (b) the Xindian River catchment.

maximum landslide area of 9.36×10^4 m^2, a total landslide area of 1.29 km^2, and a landslide-area ratio of 0.17%. For the Xindian River catchment, Typhoon Soudelor in 2015 had the largest effect, resulting in 164 landslides, a maximum landslide area of 1.17×10^5 m^2, a total landslide area of 0.65 km^2, and a landslide-area ratio of 0.132%. Only 16 landslides occurred during Typhoon Saola in 2012 and Typhoon Soulik in 2013, and the total landslide area and landslide-area ratio during Typhoon Soulik in 2013 were only 0.08 km^2 and 0.015%, respectively. In addition, the smallest maximum landslide area of 1.99×10^4 m^2 occurred during Typhoon Krosa in 2007.

Table 2 shows the average rainfall conditions of the two catchments during each typhoon event. Among those typhoon events, in the Shihmen Reservoir catchment, Typhoon Sinlaku in 2008 had the highest cumulative rainfall of 981.85 mm and the longest rainfall duration of 70 h, and Typhoon Aere had the strongest mean rainfall intensity of 21.49 mm/h. The strongest peak rainfall intensity, 70.19 mm/h, occurred during Typhoon Soulik. In the Xindian River catchment, Typhoon Sinlaku in 2008 had the highest cumulative rainfall of 1099.07 mm and the longest rainfall duration of 87 h. Typhoon Soudelor had the highest rainfall intensity; the mean rainfall intensity of that typhoon was 20.38 mm/h, and the peak rainfall intensity was 48.88 mm/h.

To establish empirical relationships between rainfall conditions and landslide-area characteristics, we compared the average rainfall conditions with the landslide-area characteristics during the typhoon events of the two catchments. Fig. 4a shows the relationship between cumulative rainfall and landslide-area ratio during typhoon events in the Shihmen Reservoir catchment. We found a good positive correlation between cumulative rainfall and landslide-area ratio ($R^2 = 0.83$), though two cases, Typhoon Sinlaku in 2008 and Typhoon Saola in 2012, did not follow that trend. Among the typhoon events, Typhoon Sinlaku in 2008 had the largest cumulative rainfall (981.85 mm) and Typhoon Saola had the third largest cumulative rainfall (849.20 mm), only slightly less than that of Typhoon Aere in 2004 (859.48 mm), in the Shihmen Reservoir catchment; however, these two typhoon events had the two lowest landslide-area ratios of 0.17% and 0.26%. This may be explained by the lack of landslide material, such as weathered soil, during the two typhoon events, which would result in a low landslide-area ratio despite the high cumulative rainfall. From Fig. 4a, we can identify two situations. When much landslide material is present, the landslide-area ratio will increase along a positive trend as the rainfall conditions increase during a typhoon period. When little landslide material is present, the landslide-area ratio will fall within a certain range of lower values regardless of rainfall conditions. We then assumed the presence of sufficient landslide material to establish empirical relationships between rainfall conditions and landslide-area characteristics and to estimate changes in landslide characteristics under climate change. Therefore, after excluding typhoons Sinlaku and Saola, we compared rainfall conditions and landslide-area characteristics for the remaining typhoon events.

Tables 3 and 4 show the Pearson correlation coefficient matrix, which compares each two factors from eight factors of rainfall conditions and landslide-area characteristics, in the Shihmen Reservoir catchment and the Xindian River catchment during each typhoon event.

Table 7
Rainfall conditions of top 10% typhoon events in the base period and the end of the 21st century.

Period	Typhoon code	Cumulative rainfall (mm)		Rainfall duration (h)		Mean rainfall intensity (mm/h)		Peak rainfall intensity (mm/h)	
		Shihmen	Xindian	Shihmen	Xindian	Shihmen	Xindian	Shihmen	Xindian
Base period	200001	1191.38	874.01	53.00	54.00	22.48	16.19	54.40	46.87
	199502	747.86	864.05	26.00	32.00	28.76	27.00	76.95	68.71
	200202	832.76	709.10	23.00	24.00	36.21	29.55	59.36	62.36
	198302	796.94	619.80	23.00	22.00	34.65	28.17	82.16	74.07
	197902	756.29	651.93	37.00	37.00	20.44	17.62	45.93	38.93
	200004	696.80	698.07	55.00	56.00	12.67	12.47	27.77	34.56
	199402	735.05	640.69	22.00	23.00	33.41	27.86	91.63	77.71
	200005	589.95	865.02	31.00	66.00	19.03	13.11	36.85	43.10
End of 21st century	209601	1154.86	1002.38	30.00	29.00	38.50	34.56	97.85	91.05
	207701	1270.84	819.97	37.00	37.00	34.35	22.16	77.26	66.72
	209005	899.61	876.73	31.00	30.00	29.02	29.22	49.81	55.05
	208301	850.86	688.80	25.00	25.00	34.03	27.55	73.49	65.61

Table 8
Landslide-area characteristics caused by top 10% typhoon events in the base period and the end of the 21st century.

Period	Typhoon code	Number of landslides		Maximum landslide area (m^2)		Total landslide area (km^2)		Landslide-area ratio (%)	
		Shihmen	Xindian	Shihmen	Xindian	Shihmen	Xindian	Shihmen	Xindian
Base period	200001	902	145	9.56×10^5	9.49×10^4	6.33	0.57	0.81	0.12
	199502	593	277	5.47×10^5	1.81×10^5	4.25	1.09	0.55	0.22
	200202	652	239	6.26×10^5	1.56×10^5	4.65	0.93	0.60	0.19
	198302	627	309	5.93×10^5	2.02×10^5	4.48	1.21	0.58	0.25
	197902	599	97	5.55×10^5	6.37×10^4	4.29	0.38	0.55	0.08
	200004	557	71	5.00×10^5	4.66×10^4	4.01	0.27	0.52	0.06
	199402	584	331	5.36×10^5	2.16×10^5	4.19	1.30	0.54	0.27
	200005	483	122	4.02×10^5	8.01×10^4	3.51	0.48	0.45	0.10
End of 21st century	209601	876	411	9.22×10^5	2.68×10^5	6.16	1.62	0.79	0.33
	207701	957	265	1.03×10^6	1.73×10^5	6.71	1.04	0.86	0.22
	209005	698	194	6.87×10^5	1.27×10^5	4.96	0.76	0.64	0.16
	208301	665	258	6.42×10^5	1.68×10^5	4.73	1.01	0.61	0.21

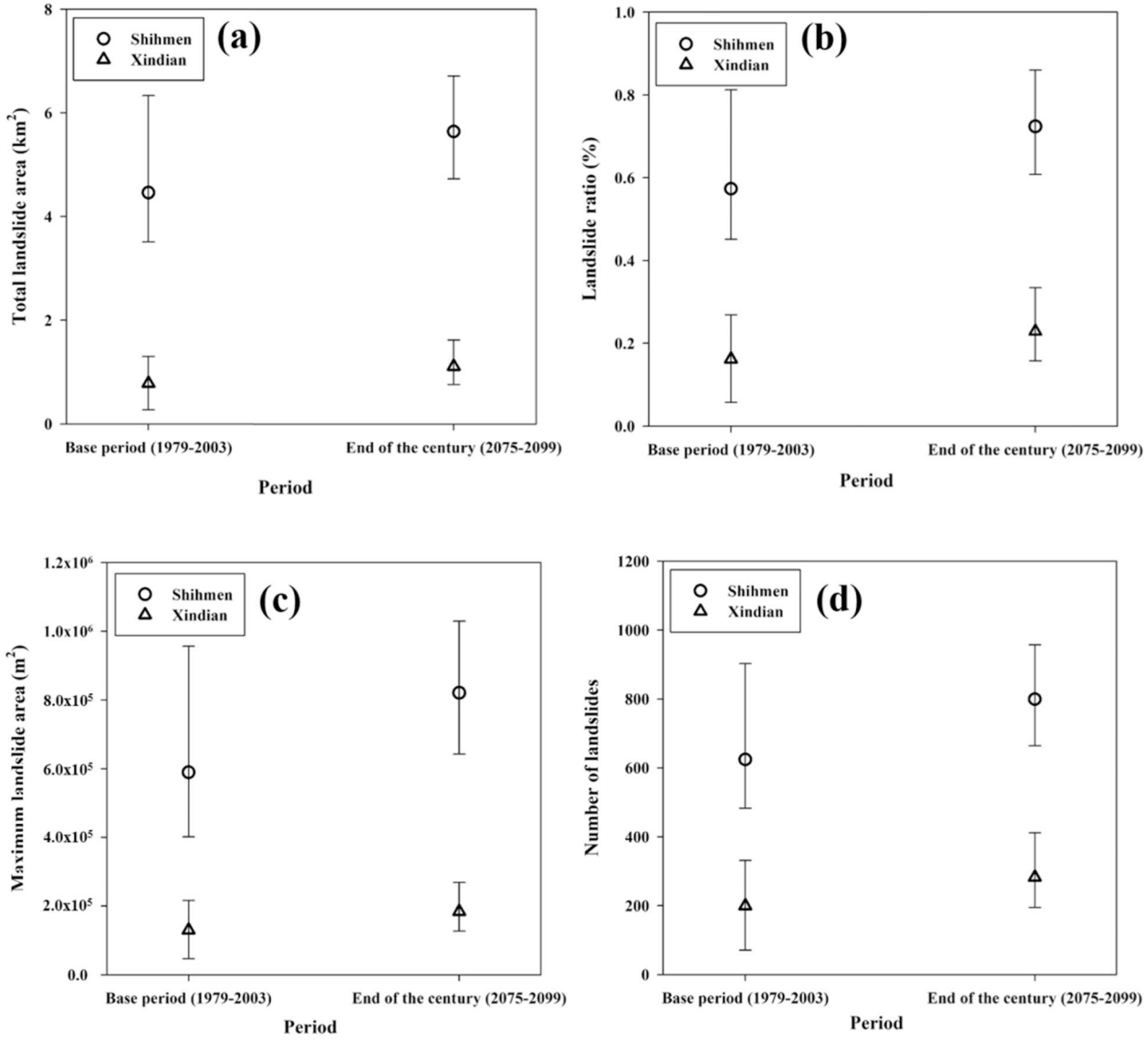

Fig. 7. Landslide-area characteristics in the base period and the end of the 21st century, including (a) total landslide area, (b) landslide-area ratio, (c) maximum landslide area, and (d) number of landslides. The upper and lower bounds are maximum and minimum values, and circles and triangles are average values.

We found that, in the Shihmen Reservoir catchment, higher correlation coefficients existed between the cumulative rainfall and landslide-area characteristics, ranging from 0.82 to 0.97 with an average of 0.90. This result indicates that it is the cumulative rainfall during a typhoon event that mainly controls the landslide-area characteristics of the Shihmen Reservoir catchment. In this catchment, higher cumulative rainfall during a typhoon event increases the total landslide area, maximum landslide area, number of landslides, and landslide-area ratio

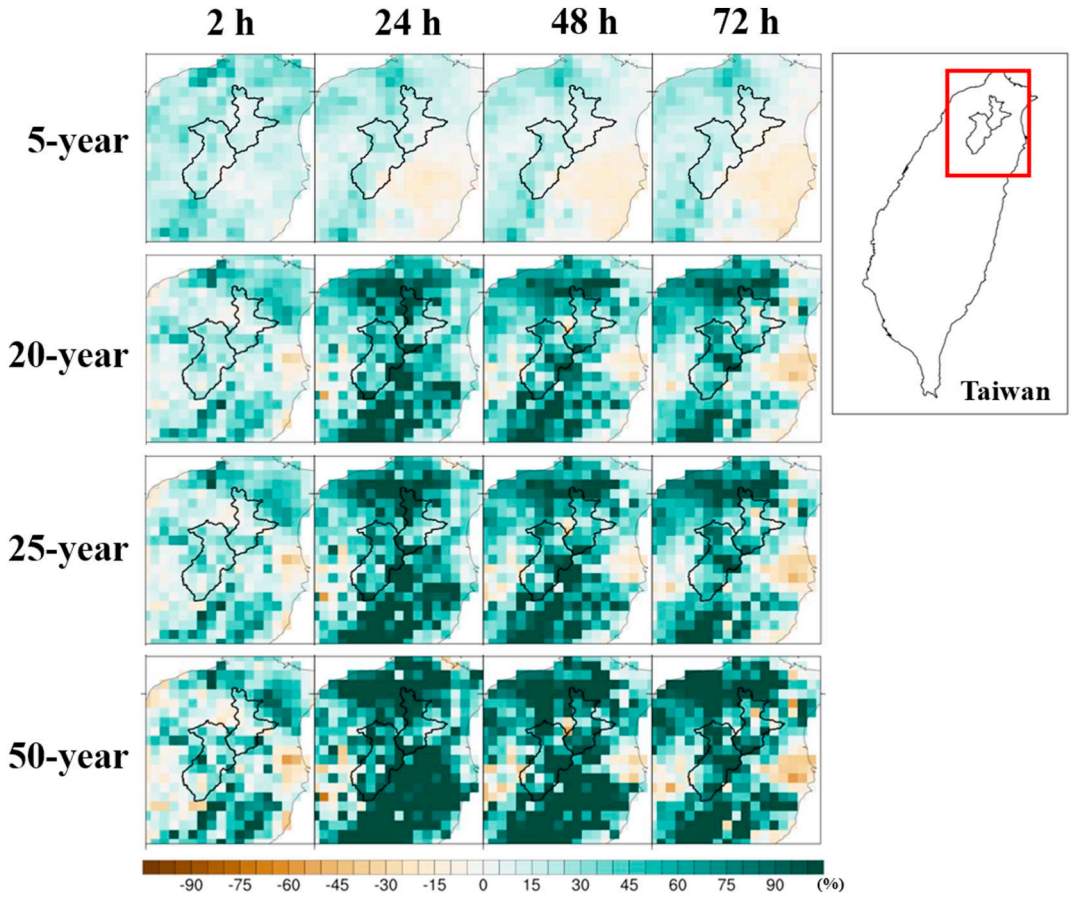

Fig. 8. Change ratio in cumulative rainfall at different recurrence intervals from different rainfall durations between the base period and the end of the 21st century. The top-right map shows the range of each map and the relative locations of the two catchments.

Table 9
Mean rainfall intensity at different recurrence intervals and different rainfall durations of the two catchments in the base period and the end of the 21st century.

Period	Recurrence interval (year)	2 h mean intensity (mm/h)		24 h mean intensity (mm/h)		48 h mean intensity (mm/h)		72 h mean intensity (mm/h)	
		Shihmen	Xindian	Shihmen	Xindian	Shihmen	Xindian	Shihmen	Xindian
Base period	5	51.34	48.88	15.11	13.06	9.39	8.36	7.02	6.35
	20	75.56	71.03	32.67	26.16	18.87	15.13	13.28	10.62
	25	80.37	75.45	37.25	29.25	21.29	16.60	14.75	11.49
	50	97.87	91.34	56.95	41.43	31.69	22.16	20.66	14.61
End of 21st century	5	58.87	58.49	16.84	16.22	10.36	9.94	7.62	7.50
	20	90.44	83.92	51.52	39.63	27.71	21.77	18.81	17.18
	25	96.99	88.93	62.72	45.96	32.91	24.81	21.99	20.01
	50	121.30	107.18	119.20	73.33	57.79	37.67	36.54	33.70

(Fig. 4a–d). In the Xindian River catchment, however, higher correlation coefficients existed between the peak rainfall intensity and landslide-area characteristics, ranging from 0.84 to 0.89 with an average of 0.87. This result indicates that it is the peak rainfall intensity during a typhoon event that mainly controls the landslide-area characteristics of the Xindian River catchment. That is, when rainfall during a typhoon event has a stronger peak rainfall intensity, the catchment will have a larger total landslide area, maximum landslide area, number of landslides, and landslide-area ratio (Fig. 4e–h). According to the results, we established empirical relationships with landslide-area characteristics using cumulative rainfall for the Shihmen Reservoir catchment and peak rainfall intensity for the Xindian River catchment as follows:

For the Shihmen Reservoir catchment:

$$A_T = 4697.3 \times E + 737287 \quad (3)$$

$$L = 0.0006 \times E + 0.0974 \quad (4)$$

$$A_M = 921.69 \times E - 141948 \quad (5)$$

$$N = 0.6969 \times E + 71.532 \quad (6)$$

For the Xindian River catchment:

$$A_T = 23764 \times I_p - 547585 \quad (7)$$

$$L = 0.0049 \times I_p - 0.1119 \quad (8)$$

$$A_M = 3924.4 \times I_p - 89062 \quad (9)$$

$$N = 6.0251 \times I_p - 137.23 \quad (10)$$

where A_T is total landslide area (m^2), L is landslide-area ratio (%), A_M is maximum landslide area (m^2), N is number of landslides, E is cumulative rainfall (mm), and I_p is peak rainfall intensity (mm/h).

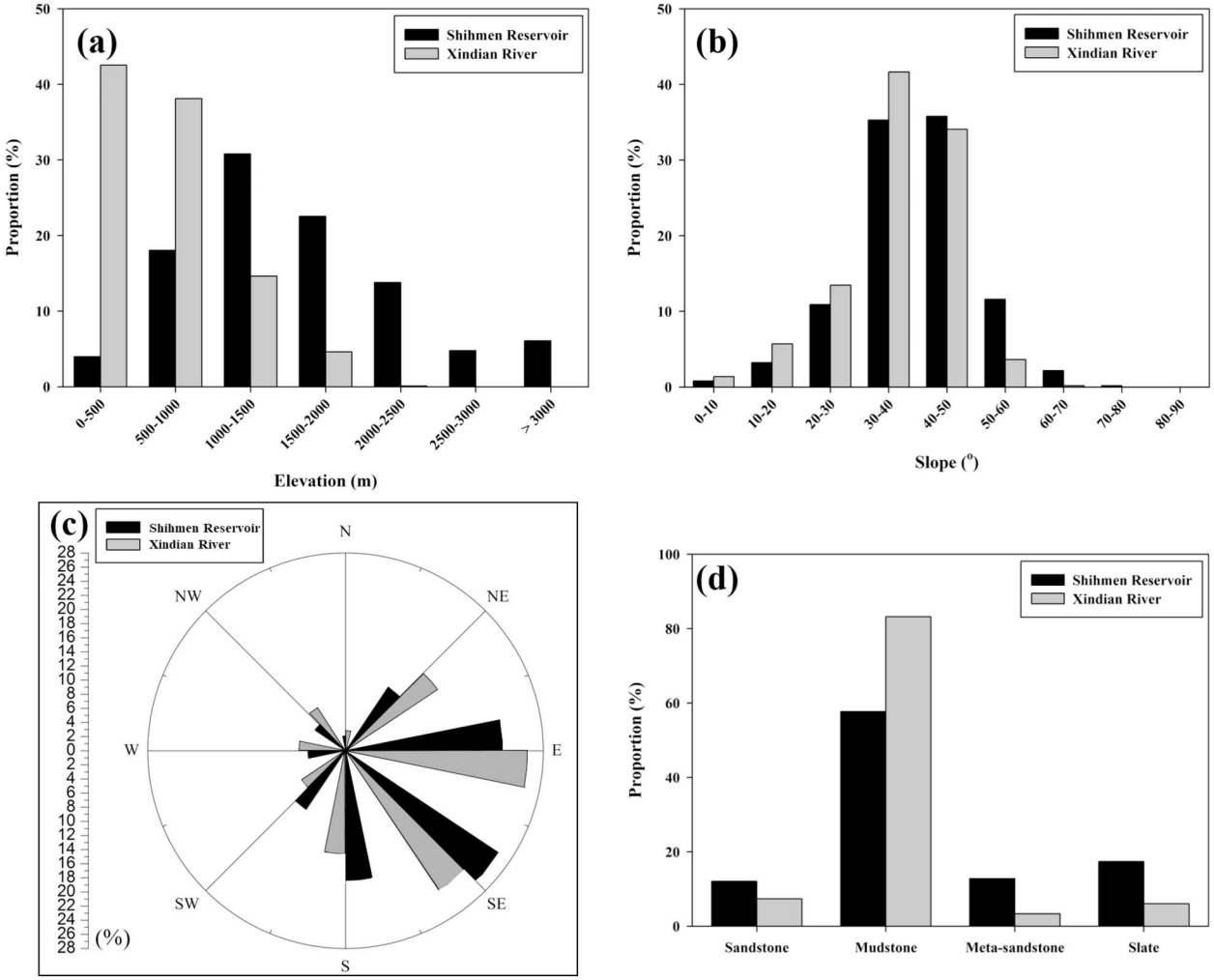

Fig. 9. Distribution of landslides of the two catchments on (a) elevation, (b) slope, (c) aspect, and (d) main lithology.

4.2. Frequency of landslides

Fig. 5 shows the results on cumulative rainfall at different recurrence intervals from different rainfall durations estimated by using the interpolated rain gauge data from 1991 to 2013. Spatially, in the Shihmen Reservoir catchment, which is located in the Xue Mountain Range, topographic rainfall easily forms on the windward side, especially during a typhoon period, and this area is also prone to landslides. As compared to the Shihmen Reservoir catchment, the Xindian River catchment has less rainfall at the 50-year recurrence interval, and the risk of landslides is relatively lower.

The total numbers of landslides induced by the historical typhoon events analyzed in this study were 3063 in the Shihmen Reservoir catchment and 458 in the Xindian River catchment. We calculated the cumulative rainfalls of the entire rainfall events for all landslides in the two catchments and excluded the highest and lowest 12.5% of the landslides. After the exclusion of these landslides, the Shihmen Reservoir catchment had 2297 landslides and the Xindian River catchment had 344 landslides. We then calculated the rainfall conditions from the beginning of the rainfall event to the occurrence of landslides (the time of peak rainfall intensity) for those landslides. As listed in Table 5, the average cumulative rainfall, rainfall duration, and mean rainfall intensity of landslides in the Shihmen Reservoir catchment were 415.67 mm, 24.63 h, and 18.70 mm/h, respectively, while those in the Xindian River catchment were 397.88 mm, 23.07 h, and 18.13 mm/h, respectively. Table 6 shows the mean rainfall intensities at different recurrence intervals from different rainfall durations of the two catchments, from which we established the *I–D* relationship for one recurrence interval. Fig. 6a shows the *I–D* relationships of landslides and rainfall conditions at different recurrence intervals in the Shihmen Reservoir catchment. The *I–D* relationship of landslides in the Shihmen Reservoir catchment is as follows:

$$I_b = 48.26 D_b^{-0.33} (5 \leq D \leq 63\ h) \quad (11)$$

This trend line is located below the rainfall conditions of the five-year recurrence interval for short rainfall duration and gradually approaches the rainfall conditions of that interval as the rainfall duration increases. Fig. 6b shows the *I–D* relationships of landslides and rainfall conditions at different recurrence intervals in the Xindian River catchment. The *I–D* relationship of landslides in the Xindian River catchment is as follows:

$$I_b = 54.17 D_b^{-0.37} (7 \leq D \leq 59\ h) \quad (12)$$

This trend line is located at the rainfall conditions of the five-year recurrence interval for short rainfall duration and gradually approaches the rainfall conditions of the 20-year recurrence interval as the rainfall duration increases. The results indicate that landslides occur in the Shihmen Reservoir catchment at a frequency of less than 5 years, but at a frequency of 5 to 20 years in the Xindian River catchment. Chen et al. (2017) pointed out that large and deep landslides usually occurred owing to long-duration rainfall, whereas small and shallow landslides occurred in a wide range of rainfall durations. According to the results of this study, small-scale landslides in the Shihmen Reservoir catchment and the Xindian River catchment occur at frequencies of less than

5 years and about 5 years respectively, and large-scale landslides occur in these two catchments at frequencies of about 5 and 20 years, respectively.

4.3. Impact of climate change on landslides

According to the climate change scenario of RCP8.5 and dynamically downscaled rainfall data, Taiwan was affected by 87 typhoons in the base period (1979–2003) and will be affected by 43 typhoons in the end of the 21st century (2075–2099). We selected eight typhoons in the base period and four typhoons in the end of the 21st century, accounting for the top 10% of the total rainfall for the Tamsui River Basin among all typhoons of the two periods, to discuss the impact of climate change on landslides. We calculated the rainfall conditions of those typhoon periods according to the definition of a rainfall event as shown in Table 7. The empirical relationships were used to estimate the landslide-area characteristics caused by the top 10% typhoon events in the base period and the end of the 21st century as shown in Table 8. Fig. 7 presents the averages from the base period to the end of the 21st century. In the Shihmen Reservoir catchment, the total landslide area will increase from 4.46 km^2 to 5.64 km^2; the landslide-area ratio, from 0.57% to 0.72%; the maximum landslide area, from 5.89×10^5 m^2 to 8.20×10^5 m^2; and the number of landslides, from 624 to 799. In terms of the change ratio, the total landslide area and landslide-area ratio will increase by about 26%; the maximum landslide area, by about 39%; and the number of landslides, by about 28%. In the Xindian River catchment, in contrast, the total landslide area will increase from 0.78 km^2 to 1.11 km^2; the landslide-area ratio, from 0.16% to 0.23%; the maximum landslide area, from 1.30×10^5 m^2 to 1.84×10^5 m^2; and the number of landslides, from 199 to 282. In terms of the change ratio, the total landslide area, landslide-area ratio, maximum landslide area, and number of landslides will increase by about 42–44%. These results are based on the assumption that the geomorphologic and geologic conditions will not change in the future. Crozier (2010) has pointed out that to assert a future climate-driven landslide response without considering the role of human activity or the geomorphic framework would lead to many uncertainties. However, Crozier (2010) also mentioned that the link between landslides and climate provides an opportunity to integrate signals over a wide area, to employ a broad range of supporting proxy information, and to provide valuable observations on mechanisms and rates of change. Our results could provide useful information to related authorities for use in making appropriate decisions and adaptations to prevent landslide hazards under climate change. Future research will be needed to consider how to incorporate future changes in geomorphologic, geologic, and vegetation conditions in order to reduce the uncertainty of assessment.

This study also used the same dynamically downscaled rainfall data in future projection to estimate the recurrence intervals of extreme rainfall for the two catchments in the base period and the end of the 21st century. Fig. 8 shows the change ratios for the base period and the end of the 21st century for cumulative rainfall at different recurrence intervals from different rainfall durations. To estimate the ratio of change in the future, we calculated the percentage of relative change: (end of century-base period) / base period × 100% (Fig. 8).

Table 9 shows the mean rainfall intensities at different recurrence intervals from different rainfall durations of the two catchments in the base period and the end of the 21st century. We found in the previous section that the trend line of the *I–D* relationship of landslides in the Shihmen Reservoir catchment was located below the rainfall conditions of the five-year recurrence interval, while that in the Xindian River catchment was located between the five- and 20-year recurrence intervals. Therefore, we further discuss changes in rainfall conditions from the base period to the end of the 21st century for the five-year recurrence interval in the Shihmen Reservoir catchment and the five- and 20-year recurrence intervals in the Xindian River catchment. In the Shihmen Reservoir catchment, the mean rainfall intensity of the five-year recurrence interval will increase by about 15% for a short duration (2 h) and 9% for a long duration (72 h); in the Xindian River catchment, the mean rainfall intensity of the five-year recurrence interval will increase by about 20% for both short and long durations, and the mean rainfall intensity of the 20-year recurrence interval will increase by about 18% for a short duration (2 h) and 62% for a long duration (72 h). The results indicate that, under the impact of climate change, the frequency of large-scale landslides will increase only slightly and that the frequency will increase mainly for small-scale landslides in the Shihmen Reservoir catchment. Conversely, the frequency of landslides will increase obviously in the Xindian River catchment, especially that of large-scale landslides, which may increase by more than half.

4.4. Causes of differences between the two catchments

This study revealed that the landslide characteristics differed in the two adjacent catchments in northern Taiwan. Here we discuss in more detail the topographic and geologic conditions of the two catchments. We can find from Fig. 2 that despite many similarities between the two catchments, the Shihmen Reservoir catchment is an area with high-relief topography, while the Xindian River catchment is an area with relatively gentle topography. Fig. 9 shows the distribution of landslides on topographical and geological conditions of the two catchments. In terms of elevation, proportions of landslides at elevation ranges of 0–500 m and 500–1000 m are higher in the Xindian River catchment (42.55% and 38.12%) than those in the Shihmen Reservoir catchment (3.99% and 18.04%). On the other hand, those at elevation ranges of 1000–1500 m and 1500–2000 m are higher in the Shihmen Reservoir catchment (30.80% and 22.54%) than those in the Xindian River catchment (14.63% and 4.61%). Some landslides (10.85%) in the Shihmen Reservoir catchment also occurred at elevations of > 2500 m (Fig. 9a). Concerning slope, both catchments are similar in that most landslides occurred at slope ranges of 30–40° and 40–50°, 35.29% and 35.80% in the Shihmen Reservoir catchment, and 41.64% and 34.06% in the Xindian River catchment respectively. However, in the slope bins of 10° interval, proportions of landslide distribution for each bin from 0 to 40° are higher in the Xindian River catchment than those in the Shihmen Reservoir catchment; while it is opposite for slope bins > 40° (Fig. 9b). Most landslides in both catchments occurred for the slope aspects of E, SE, and S (66.51% in the Shihmen Reservoir catchment and 62.06% in the Xindian River catchment; Fig. 9c). Among lithology types, the landslide distribution has the highest proportion for mudstone (57.69% in the Shihmen Reservoir catchment and 83.18% in the Xindian River catchment), and similar lower proportions for other lithologies (Fig. 9d). Landslides in the Shihmen Reservoir catchment tend to occur on areas with higher elevations and steeper slopes than those in the Xindian River catchment.

An area with high-relief topography, such as the Shihmen Reservoir catchment, is relatively prone to landslides. The landslide-area ratio during past typhoon events averaged 0.4% (Table 1), and landslides mainly occurred under rainfall conditions of less than the five-year recurrence interval (Fig. 5a). In such areas, the cumulative rainfall is a key factor controlling landslide-area characteristics. Soil water content and groundwater level will be higher as the cumulative rainfall increases, and the combination of these higher levels with high-relief topography will lead to landslides. The size of each landslide will be determined by the soil water content and groundwater level. In contrast, an area with gentle topography, such as the Xindian River catchment, is less prone to landslides. The landslide-area ratio during past typhoon events averaged 0.05% (Table 1), and landslides mainly occurred under the rainfall conditions of the five- to 20-year recurrence intervals (Fig. 5b). In such areas, the rainfall intensity is a key factor controlling landslide-area characteristics. The main type of landslide in such areas is shallow landslides, which are caused by the erosion of surface materials; this erosion depends on the rainfall intensity. In addition, we can find from the estimation of the impact of climate change

on landslide characteristics that in areas less prone to landslides at present, both landslide-area characteristics and landslide frequency will increase under climate change. The reason may be increases in the probability of the occurrence of a strong typhoon and in the rainfall intensity during a typhoon event in a changing climate (Emanuel, 2005; Webster et al., 2005; Tu et al., 2009). Although this study has provided a possible changes of landslide characteristics under ongoing climate change, the future is full of uncertainties with additional impacts from changes in human activities and the efficiency of carbon reduction, which can lead to different possibilities. It is essential to incorporate more climate change scenarios in the future work and use ensemble methods to obtain more reliable results.

5. Conclusions

This study used landslides triggered by historical typhoon events to establish the empirical relationship between rainfall conditions and landslide characteristics and identified the frequency of landslides for two adjacent catchments in northern Taiwan. The Shihmen Reservoir catchment has high-relief topography, and it is highly prone to landslides at present. During past typhoon events, the average landslide-area ratio was 0.4%, and landslides mainly occurred under rainfall conditions of less than the five-year recurrence interval. In this catchment, the cumulative rainfall is a key factor controlling landslide characteristics. In contrast, the Xindian River catchment has gentle topography and is less prone to landslides at present. During past typhoon events, the average landslide-area ratio was 0.05%, and landslides mainly occurred under rainfall conditions of the five- to 20-year recurrence intervals. In this catchment, the rainfall intensity is a key factor controlling landslide characteristics.

According to the climate change scenario of representative concentration pathways 8.5 (RCP8.5) and dynamically downscaled rainfall data in Taiwan, from the base period to the end of the 21st century, the total landslide area and landslide-area ratio in the Shihmen Reservoir catchment will increase by about 26%; the maximum landslide area, by about 39%; and the number of landslides, by about 28%. In the Xindian River catchment, the total landslide area, landslide-area ratio, maximum landslide area, and number of landslides will increase by about 42–44%. For the same time period, the mean rainfall intensity of the five-year recurrence interval in the Shihmen Reservoir catchment will increase by about 15% for a short duration and 9% for a long duration from the base period to the end of the 21st century. In the Xindian River catchment, the mean rainfall intensity of the five-year recurrence interval will increase by about 20% for both short and long durations, and the mean rainfall intensity of the 20-year recurrence interval will increase by about 18% for a short duration and 62% for a long duration. These predictions indicate that, under the effects of climate change, both the landslide severity and the landslide frequency will increase more in the Xindian River catchment than in the Shihmen Reservoir catchment. The reason may be increases in the probability of the occurrence of a strong typhoon and in the rainfall intensity during a typhoon event in a changing climate.

Acknowledgments

We would like to thank the theme C of the Program for Risk Information on Climate Change of Japan (SOUSEI-C) for providing the MRI-AGCM data. We are also very grateful to Dr. Ai-Ti Chen in the Department of Geosciences, National Taiwan University, discussing with us and providing many helpful comments. This research was supported by the Taiwan Climate Change Projection and Information Platform (TCCIP; MOST106-2621-M-865-001).

References

Aleotti, P., 2004. A warning system for rainfall-induced shallow failures. Eng. Geol. 73, 247–265.
Ayalew, L., Yamagishi, H., 2005. The application of GIS-based logistic regression for landslide susceptibility mapping in the Kakuda-Yahiko Mountains, Central Japan. Geomorphology 65, 15–31.
Brunetti, M.T., Peruccacci, S., Rossi, M., Luciani, S., Valigi, D., Guzzetti, F., 2010. Rainfall thresholds for the possible occurrence of landslides in Italy. Nat. Hazards Earth Syst. Sci. 10, 447–458.
Caine, N., 1980. The rainfall intensity–duration control of shallow landslides and debris flows. Geogr. Ann., Ser. A 62, 23–27.
Chang, C.W., Lin, P.S., Tsai, C.L., 2011. Estimation of sediment volume of debris flow caused by extreme rainfall in Taiwan. Eng. Geol. 123, 83–90.
Chanson, H., 1998. Extreme reservoir sedimentation in Australia: a review. Int. J. Sediment Res. 13, 55–63.
Chen, H., Su, D.I., 2001. Geological factors for hazardous debris flow in Hoser, central Taiwan. Environ. Geol. 40, 1114–1124.
Chen, H., Chen, R.H., Lin, M.L., 1999. Initiative anatomy of Tungmen debris flow, eastern Taiwan. Environ. Eng. Geosci. 5, 459–473.
Chen, C.W., Saito, H., Oguchi, T., 2015. Rainfall intensity–duration conditions for mass movements in Taiwan. Prog. Earth Planet Sci. 2, 14.
Chen, C.W., Oguchi, T., Hayakawa, Y.S., Saito, H., Chen, H., 2017. Relationship between landslide size and rainfall conditions in Taiwan. Landslides 14, 1235–1240.
Chiang, S.H., Chang, K.T., 2009. Application of radar data to modeling rainfall-induced landslides. Geomorphology 103, 299–309.
Chou, H.T., Lee, C.F., Lo, C.M., 2017. The formation and evolution of a coastal alluvial fan in eastern Taiwan caused by rainfall-induced landslides. Landslides 14, 109–122.
Chuang, S.C., Chen, H., Lin, G.W., Lin, C.W., Chang, C.P., 2009. Increase in basin sediment yield from landslides in storms following major seismic disturbance. Eng. Geol. 103, 59–65.
Crozier, M.J., 1999. Prediction of rainfall-triggered landslides: a test of the antecedent water status model. Earth Surf. Process. Landf. 24, 825–833.
Crozier, M.J., 2010. Deciphering the effect of climate change on landslide activity: a review. Geomorphology 124, 260–267.
Dadson, S.J., Hovius, N., Chen, H., Dade, W.B., Hsieh, M.L., Willett, S.D., Hu, J.C., Horng, M.J., Chen, M.C., Stark, C.P., Lague, D., Lin, J.C., 2003. Links between erosion, runoff variability and seismicity in the Taiwan orogeny. Nature 426, 648–651.
Dahal, R., Hasegawa, S., 2008. Representative rainfall thresholds for landslides in the Nepal Himalaya. Geomorphology 100, 429–443.
Emanuel, K., 2005. Increasing destructiveness of tropical cyclones over the past 30 years. Nature 436, 686–688.
Glade, T., Crozier, M., Smith, P., 2000. Applying probability determination to refine landslide-triggering rainfall thresholds using an empirical "Antecedent Daily Rainfall Model". Pure Appl. Geophys. 157, 1059–1079.
Guzzetti, F., Carrara, A., Cardinali, M., Reichenbach, P., 1999. Landslide hazard evaluation: a review of current techniques and their application in a multi-scale study, Central Italy. Geomorphology 31, 181–216.
Guzzetti, F., Peruccacci, S., Rossi, M., Stark, C., 2007. Rainfall thresholds for the initiation of landslides in central and southern Europe. Meteorog. Atmos. Phys. 98, 239–267.
Guzzetti, F., Peruccacci, S., Rossi, M., Stark, C., 2008. The rainfall intensity–duration control of shallow landslides and debris flows: an update. Landslides 5, 3–17.
Ho, C.S., 1986. A synthesis of the geologic evolution of Taiwan. Tectonophysics 125, 1–16.
Hsu, H.H., Chou, C., Wu, Y.C., Lu, M.M., Chen, C.T., Chen, Y.M., 2011. Climate Change in Taiwan: Scientific Report 2011 (Summary). National Science Council, Taipei, Taiwan.
Hu, T.J., Wang, H.W., Lee, H.Y., 2007. Assessment of environmental conditions of Nan-Shih stream in Taiwan. Ecol. Indic. 7, 430–441.
Huang, J.C., Lin, C.C., Chan, S.C., Lee, T.Y., Hsu, S.C., Lee, C.T., Lin, J.C., 2012. Stream discharge characteristics through urbanization gradient in Danshui River, Taiwan: perspectives from observation and simulation. Environ. Monit. Assess. 184, 5689–5703.
Iida, T., 2004. Theoretical research on the relationship between return period of rainfall and shallow landslides. Hydrol. Process. 18, 739–756.
IPCC, 2007. Climate change 2007: The physical science basis. In: Summary for Policymakers. Contribution of Working Group I to the Fourth Assessment Report. The Intergovernmental Panel on Climate Change.
Johns, T.C., Carnell, R.E., Crossley, J.F., Gregory, J.M., Mitchell, J.F., Senior, C.A., Tett, S.F.B., Wood, R.A., 1997. The second Hadley Centre coupled ocean-atmosphere GCM: model description, spinup and validation. Clim. Dyn. 13, 103–134.
Khan, Y.A., Lateh, H., Baten, M.A., Kamil, A.A., 2012. Critical antecedent rainfall conditions for shallow landslides in Chittagong City of Bangladesh. Environ. Earth Sci. 67, 97–106.
Kharin, V.V., Zwiers, F.W., 2005. Estimating extremes in transient climate change simulations. J. Clim. 18, 1156–1173.
Larsen, M., Simon, A., 1993. A rainfall intensity–duration threshold for landslides in a humid-tropical environment: Puerto Rico. Geogr. Ann., Ser. A 75, 13–23.
Lin, G.W., Chuang, S.C., Yuan, C.W., Chen, Y.H., Chen, H., 2007. Relationship between landslide and sediment discharge in the river catchments of central and north Taiwan. J. Eng. Environ. 19, 81–95 (in Chinese with English abstract).
Lin, G.W., Chen, H., Petley, D.N., Horng, M.J., Wu, S.J., Chuang, B., 2011. Impact of rainstorm-triggered landslides on high turbidity in a mountain reservoir. Eng. Geol. 117, 97–103.
Liu, S.H., Lin, C.W., Tseng, C.M., 2013. A statistical model for the impact of the 1999 Chi-Chi earthquake on the subsequent rainfall-induced landslides. Eng. Geol. 156, 11–19.
Melchiorre, C., Frattini, P., 2012. Modelling probability of rainfall-induced shallow landslides in a changing climate, Otta, Central Norway. Clim. Chang. 113, 413–436.
Migoń, P., Jancewicz, K., Różycka, M., Duszyński, F., Kasprzak, M., 2017. Large-scale

slope remodelling by landslides–geomorphic diversity and geological controls, Kamienne Mts., Central Europe. Geomorphology 289, 134–151.
Mizuta, R., Yoshimura, H., Murakami, H., Matsueda, M., Endo, H., Ose, T., Kamiguchi, K., Hosaka, M., Sugi, M., Yukimoto, S., Kusunoki, S., Kitoh, A., 2012. Climate simulations using MRI-AGCM3.2 with 20-km grid. J. Meteorol. Soc. Jpn. 90A, 233–258.
Mizuta, R., Arakawa, O., Ose, T., Kusunoki, S., Endo, H., Kitoh, A., 2014. Classification of CMIP5 future climate responses by the tropical sea surface temperature changes. SOLA 10, 167–171.
Murakami, H., Wang, Y., Yoshimura, H., Mizuta, R., Sugi, M., Shindo, E., Adachi, Y., Yukimoto, S., Hosaka, M., Kusunoki, S., Ose, T., Kitoh, A., 2012. Future changes in tropical cyclone activity projected by the new high-resolution MRI-AGCM. J. Clim. 25, 3237–3260.
Murakami, H., Hsu, P.C., Arakawa, O., Li, T., 2014. Influence of model biases on projected future changes in tropical cyclone frequency of occurrence. J. Clim. 27, 2159–2181.
Oku, Y., Yoshino, J., Takemi, T., Ishikawa, H., 2014. Assessment of heavy rainfall-induced disaster potential based on an ensemble simulation of Typhoon Talas (2011) with controlled track and intensity. Nat. Hazards Earth Syst. Sci. 14, 2699–2709.
Paudel, U., Oguchi, T., Hayakawa, Y., 2016. Multi-resolution landslide susceptibility analysis using a DEM and random forest. Int. J. Geosci. 7, 726.
Roble, R.G., Ridley, E.C., 1994. A thermosphere-ionosphere-mesosphere-electrodynamics general circulation model (TIME-GCM): equinox solar cycle minimum simulations (30–500 km). Geophys. Res. Lett. 21, 417–420.
Saito, H., Matsuyama, H., 2012. Catastrophic landslide disasters triggered by record-breaking rainfall in Japan: their accurate detection with normalized soil water index. SOLA 8, 81–84.
Saito, H., Matsuyama, H., 2015. Probable hourly precipitation and soil water index for 50-yr recurrence interval over the Japanese Archipelago. SOLA 11, 118–123.
Saito, H., Nakayama, D., Matsuyama, H., 2010. Relationship between the initiation of a shallow landslide and rainfall intensity–duration thresholds in Japan. Geomorphology 118, 167–175.
Shieh, S.L., 2000. User's Guide for Typhoon Forecasting in the Taiwan Area (VIII). Central Weather Bureau, Taipei.
Shou, K.J., Hong, C.Y., Wu, C.C., Hsu, H.Y., Fei, L.Y., Lee, J.F., Wei, C.Y., 2011. Spatial and temporal analysis of landslides in Central Taiwan after 1999 Chi-Chi earthquake. Eng. Geol. 123, 122–128.
Taiwan Water Resources Agency, 2013. Annual Report of Taiwan Hydrology in 2012. Taiwan Water Resources Agency, Executive Yuan, Taiwan.
Tao, T., Chocat, B., Liu, S., Xin, K., 2009. Uncertainty analysis of interpolation methods in rainfall spatial distribution–a case of small catchment in Lyon. J. Environ. Prot. 1, 50–58.
Teng, L.S., 1990. Geotectonic evolution of late Cenozoic arc-continent collision in Taiwan. Tectonophysics 183, 57–76.
Tu, J.Y., Chou, C., Chu, P.S., 2009. The abrupt shift of typhoon activity in the vicinity of Taiwan and its association with western North Pacific–East Asian climate change. J. Clim. 22, 3617–3628.
Turkington, T., Remaître, A., Ettema, J., Hussin, H., van Westen, C., 2016. Assessing debris flow activity in a changing climate. Clim. Chang. 137, 293–305.
Uchiogi, T., 1971. Landslides due to one continual rainfall. Journal of the Japan Society of Erosion. Control. Eng. 23, 21–34 (in Japanese).
Varnes, D.J., 1978. Slope movement types and processes chapter 2. In: Schuster, R.L., Krizek, R.J. (Eds.), Landslides, Analysis and Control. vol. 176. National Academy of Sciences, Transport Research Board Special Report, pp. 11–33.
Webster, P.J., Holland, G.J., Curry, J.A., Chang, H.R., 2005. Changes in tropical cyclone number, duration, and intensity in a warming environment. Science 309, 1844–1846.
Yalcin, A., 2008. GIS-based landslide susceptibility mapping using analytical hierarchy process and bivariate statistics in Ardesen (Turkey): comparisons of results and confirmations. Catena 72, 1–12.
Zhu, J., Ding, J., Liang, J., 2011. Influences of the Wenchuan Earthquake on sediment supply of debris flows. J. Mt. Sci. 8, 270.